

# **Investigation of droplet-mediated sensible and latent heat fluxes in a turbulent air flow over a waved water surface by direct numerical simulation**

Oleg A. Druzhinin

Institute of Applied Physics, Russian Acad. Sci., Nizhny Novgorod, Russia

## **Summary**

The objective of the present study is to investigate sensible and latent heat transfer mediated by evaporating saline droplets in a turbulent air flow over a waved water surface by performing direct numerical simulation. Equations of the air-flow velocity, temperature and humidity are solved simultaneously with the two-way-coupled equations of individual droplets coordinates and velocities, temperatures and masses. Two different cases of air and water surface temperatures,  $T_a = 27^0C, T_s = 28^0C$ , and  $T_a = -10^0C, T_s = 0^0C$ , are considered and conditionally termed as "tropical cyclone" (TC) and "polar low" (PL) conditions, respectively. Droplets-mediated sensible and latent heat fluxes,  $Q_S$  and  $Q_L$ , are integrated along individual droplets Lagrangian trajectories and evaluated as distributions over droplet diameter at injection,  $d$ , and also obtained as Eulerian, ensemble-averaged fields. The results show that under TC-conditions, the sensible heat flux from droplets to air is negative whereas the latent heat flux is positive, and thus droplets cool and moisturize the carrier air. On the other hand, under PL-conditions,  $Q_S$  and  $Q_L$  are both positive, and  $Q_L$  – contribution is significantly reduced as compared to  $Q_S$  - contribution. Thus in this case, droplets warm up the air. In both cases, the droplet-mediated enthalpy flux,  $Q_S + Q_L$ , is positive, vanishes for sufficiently small droplets (with diameters  $d \leq 150 \mu\text{m}$ ) and further increases with  $d$ . The results also show that the net fluxes are reduced with increasing wave slope.

## Schematic of DNS

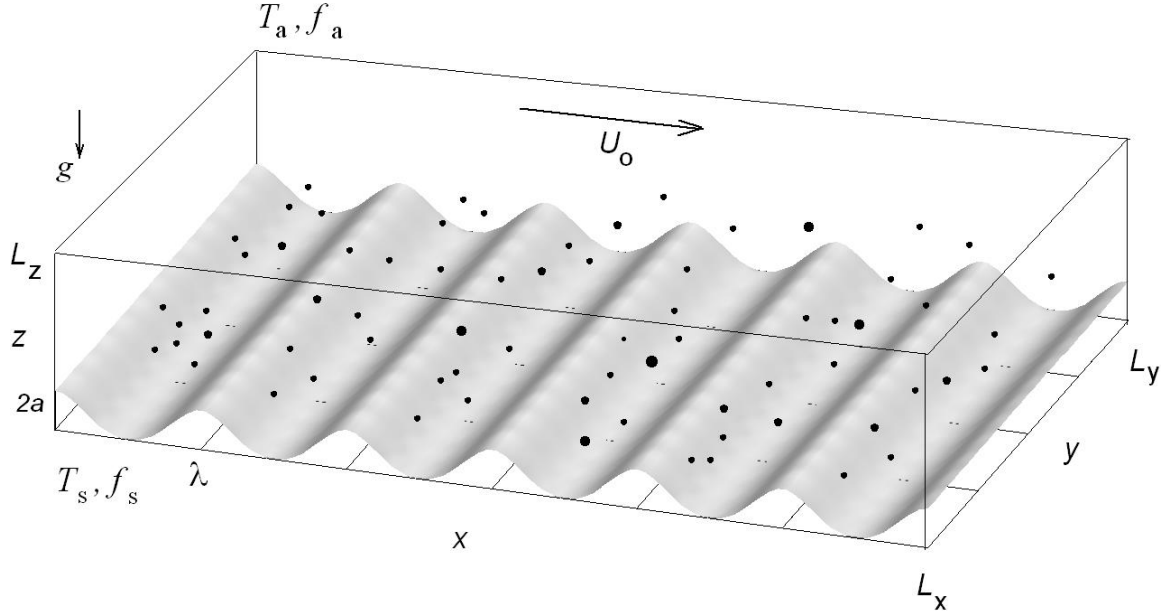


**Fig 1** Schematic of DNS:  $L_{x,y,z}$  are the domain sizes in the horizontal ( $x$ ), spanwise ( $y$ ), and vertical ( $z$ ) directions;  $a$  and  $\lambda$  are the surface water wave amplitude and length;  $T_s, f_s$  and  $T_a, f_a$  are the temperature and fractional relative humidity at the water surface and at the top boundary, respectively;  $U_0$  the bulk velocity of the air-flow, and  $g$  is the acceleration due to gravity. Droplets are denoted by black dots. Symbols sizes are not to scale.

Two-dimensional,  $x$ -periodic water surface wave with amplitude  $a$  and wavelength  $\lambda$  is prescribed and considered unaffected by either air-flow or droplets. DNS is performed in a reference frame moving with the wave phase velocity,  $c$ . No-slip (Dirichlet) boundary condition is prescribed for the air velocity at the bottom boundary, where it coincides with the velocity in the surface wave, and at the top boundary plane moving in the  $x$ -direction with bulk velocity,  $U_0$ . The air flow is assumed to be periodic in the  $x$ - and  $y$ -directions. Two different cases of air and water surface temperatures,  $T_a = 27^0C$ ,  $T_s = 28^0C$ , and  $T_a = -10^0C$ ,  $T_s = 0^0C$ , are studied and conditionally termed as "tropical cyclone" (TC) and "polar low" (PL) conditions, respectively. In both cases, the relative humidity is prescribed as  $f_a = 0.8$  and  $f_s = 0.98$  at the top and surface-wave boundaries, respectively. The wave celerity is prescribed to be sufficiently small,  $c/U_0 = 0.05$ , which is characteristic of "slow" waves as compared to the wind.

## Numerical procedure

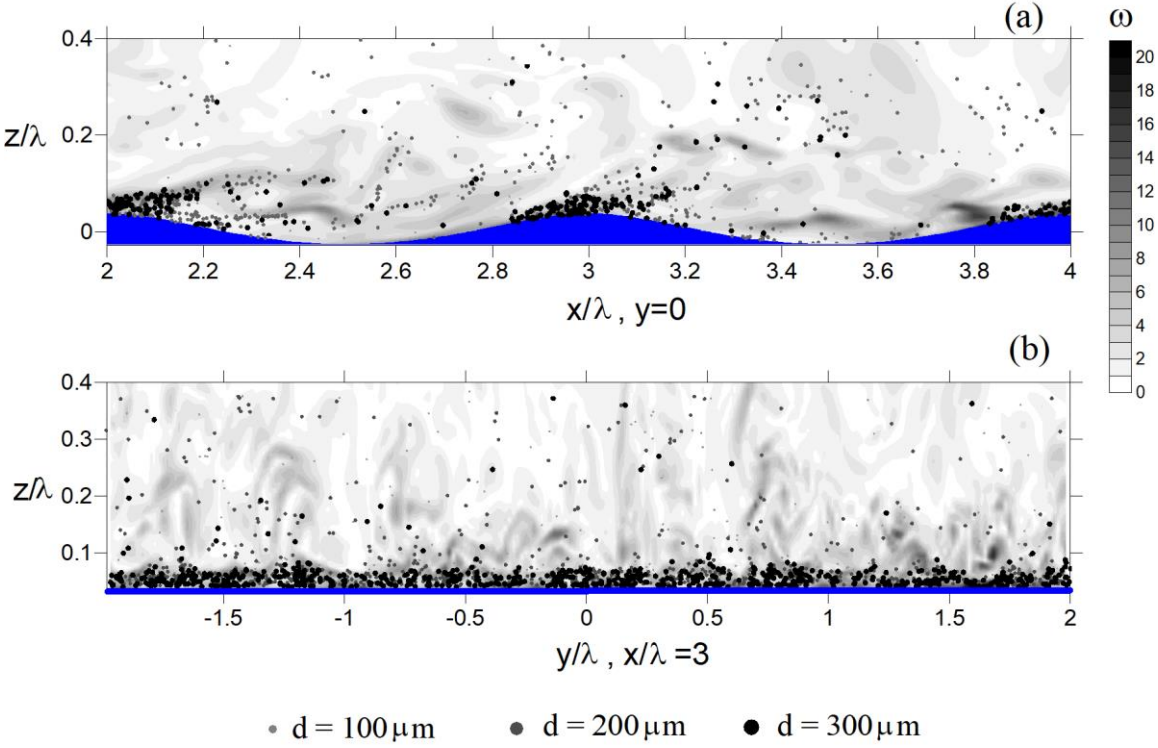


**Fig 2** Instantaneous distribution of the vorticity modulus,  $\omega$ , (grey scale), and droplets locations (symbols) in DNS at  $tU_0/\lambda = 300$  in central ( $x,z$ ) (a) and ( $y,z$ ) (b) planes. Only the droplets with diameters  $d \approx 100\mu\text{m}$  (with ratio  $V_s/\kappa u_* \approx 0.25$ ),  $d \approx 200\mu\text{m}$  ( $V_s/\kappa u_* \approx 1$ ) and  $d \approx 300\mu\text{m}$  ( $V_s/\kappa u_* \approx 2.25$ ), represented by symbols of different color and size, are shown. Symbols sizes are not to scale. Wave slope  $ka = 0.2$ , initial droplet mass fraction  $C_0 = 0.038$ .

The equations for the carrier air-flow (momentum, continuity, temperature and humidity) are solved in a Eulerian frame simultaneously with the Lagrangian equations of individual droplets coordinates and velocities, and temperatures and masses, taking into accounts the feedback for all fields by the

droplets. The air-flow bulk Reynolds number  $\text{Re} = \frac{U_0\lambda}{\nu_a}$  is set equal to  $\text{Re} = 15000$ . The friction

Reynolds number equals  $\text{Re}_* = u_*\lambda/\nu_a \approx 500$ , and is sufficiently large and allows a fully-developed turbulent air-flow.  $N_d = 3 \cdot 10^6$  poly-disperse droplets are injected in the vicinity of the water surface and randomly distributed at upwind wave slopes in the vicinity of the wave crests with velocities and temperatures equal to those of water particles in the surface wave.

## Fluxes evaluation

The sensible heat flux is proportional to the product of the instantaneous difference of the air temperature at the n-th drop location,  $T(r^n)$ , and the droplet temperature,  $T_n$ , and the thermal conductivity coefficient,  $\kappa$ , (Pruppacher & Klett, 1978):

$$Q_S^n = 2\pi c_a \rho_a \kappa d_n (T_n - T(r^n)) (1 + 0.25 \text{Re}_n^{0.5}), \quad (1)$$

where  $c_a$  is the specific heat of air. The latent heat flux is proportional to the rate of change of droplet mass and the latent heat of evaporation,  $L_v$ :

$$Q_L^n = -L_v \frac{dm_n}{dt} = 2\pi D L_v d_n (\rho_{sat,n}^v - \rho_a q(r^n)) (1 + 0.25 \text{Re}_n^{0.5}). \quad (2)$$

Sensible and latent heat fluxes, Eqs. (1) and (2), include corrections due to finite droplet Reynolds number,  $\text{Re}_n$ , caused by the ventilation effects. The saturated vapor density at the droplet surface,  $\rho_{sat,n}^v$ , in Eq. (2) is evaluated as (Pruppacher & Klett, 1978, Andreas, 1989):

$$\rho_{sat,n}^v = \rho_{sat}^v \exp \left[ L_v M_w \frac{T_n - T}{T_n T} + \frac{4\sigma M_w T}{d_n \rho_w R_g T_n} - \frac{2\Phi m_{ns} M_w}{M_s (m_n - m_{ns})} \right], \quad (3)$$

where the saturation vapor density over a flat, pure-water surface is (cf. Buck, 1981):

$$\rho_{sat}^v = \frac{M_w}{R_g T} \left( 1 + 3.46 \times 10^{-6} P_a \right) \exp \left( \frac{17.502(T - 273.15)}{T - 32.18} \right). \quad (4)$$

In Eq.(3),  $T \equiv T(r^n)$  is the air temperature at the location of  $n$ -th droplet,  $r^n$ , and  $T_n$  is the droplet temperature;  $q(r^n)$  the specific humidity at  $n$ -th droplet location;  $\sigma$  is the surface tension of a flat surface of water with the same salinity and temperature as the droplet solution;  $\Phi$  the practical osmotic coefficient of the droplet;  $M_s$  and  $M_w$  are molecular weights of salt and water, respectively;  $\rho_w$  the fresh water density;  $R_g$  the universal gas constant ; and  $m_{ns}$  is a mass of salt in the droplet solution. The latter remains constant for each drop during the simulation and is defined by the initially-prescribed salinity of sea water (34 psu) and droplet volume. The temperatures in Eqs. (3),(4) are in Kelvins.

## Droplets Lagrangian dynamics: TC case

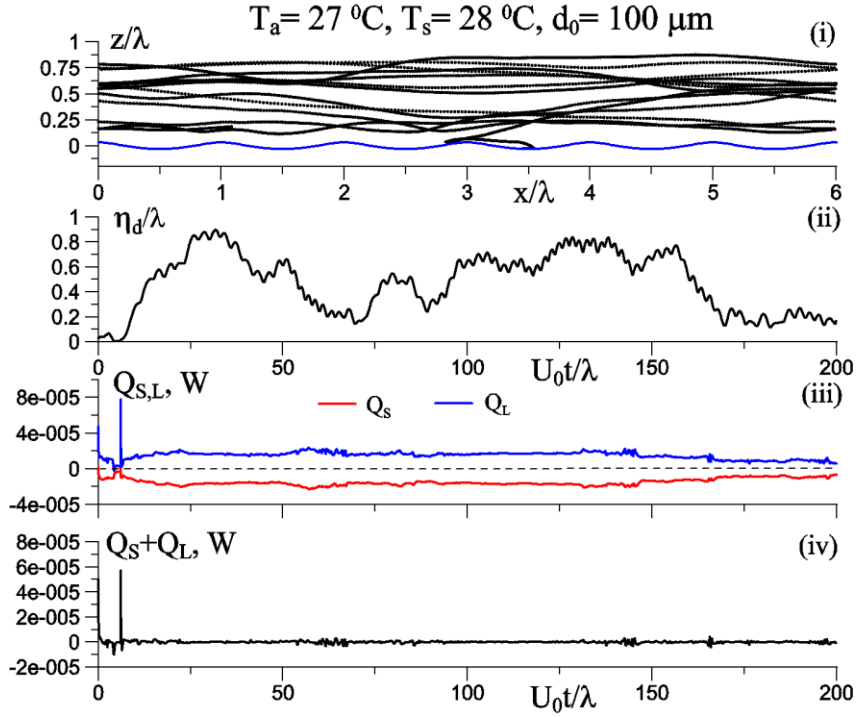


**Fig 3** The side view of the trajectory of a droplet with initial diameter  $d_0 = 100 \mu\text{m}$  in DNS with TC-conditions, (i); the height of the droplet above water surface,  $\eta_d$ , (ii); sensible and latent heat fluxes from droplet to air,  $Q_s$  and  $Q_L$ , (iii); the enthalpy flux,  $Q_s + Q_L$ , (iv); wave slope  $ka = 0.2$ .

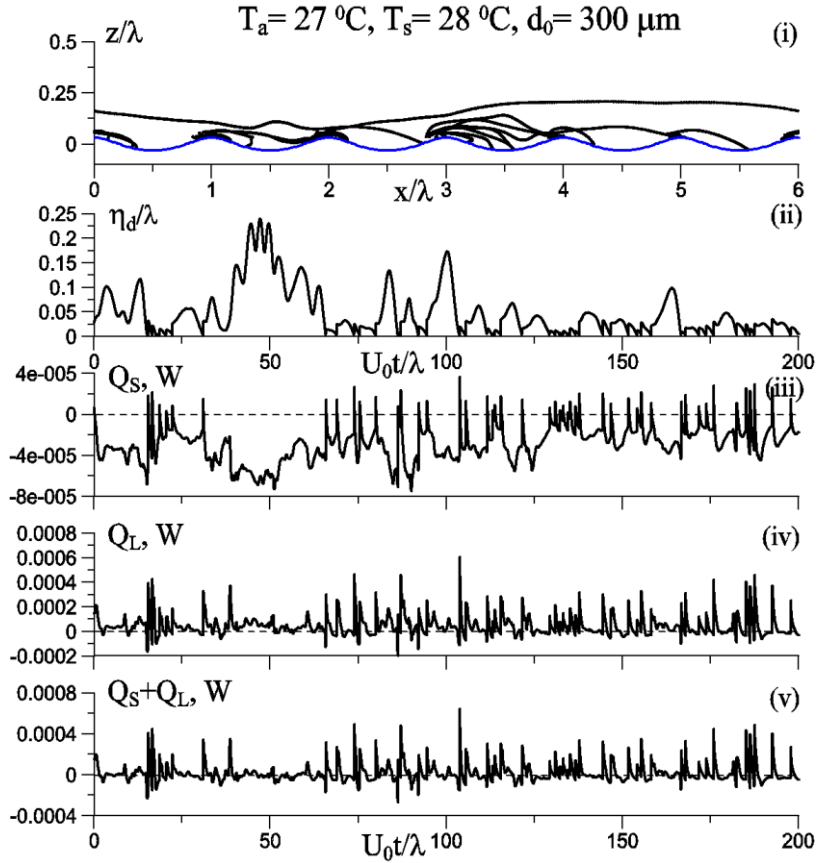


**Fig 4** The side view of the trajectory of a droplet with initial diameter  $d_0 = 300 \mu\text{m}$  in DNS with TC-conditions, (i); the height of the droplet above water surface,  $\eta_d$ , (ii); sensible and latent heat fluxes from droplet to air,  $Q_s$  and  $Q_L$ , (iii) and (iv), respectively; and the enthalpy flux,  $Q_s + Q_L$ , (v).

## Droplets Lagrangian dynamics: PL case

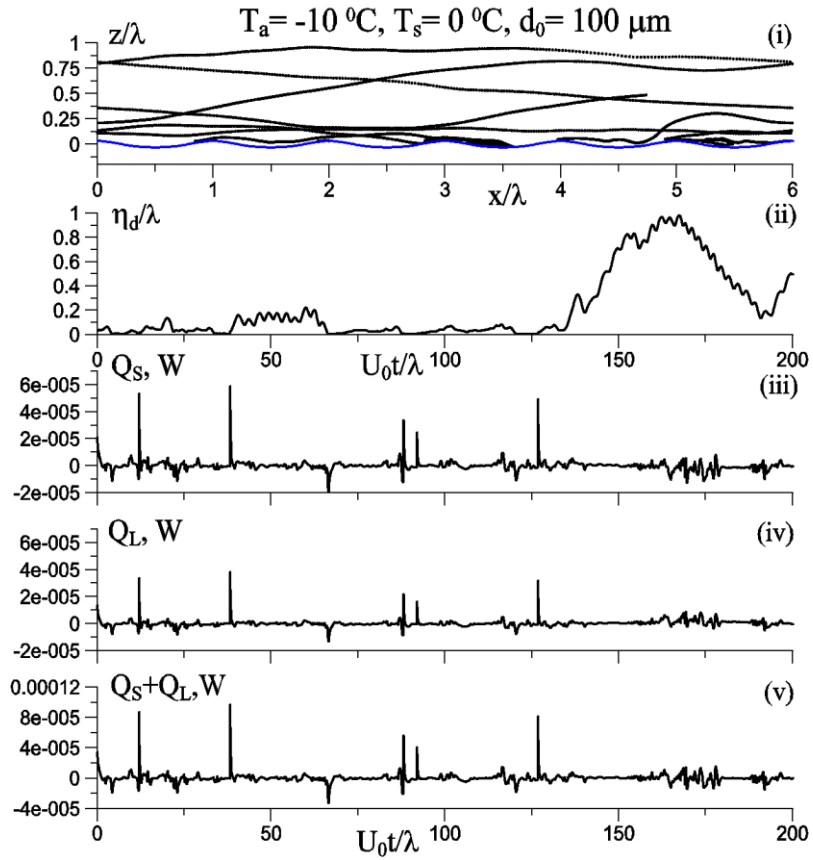


**Fig 5** The side view of the trajectory of a droplet with initial diameter  $d_0 = 100 \mu\text{m}$  in DNS with PL-conditions.

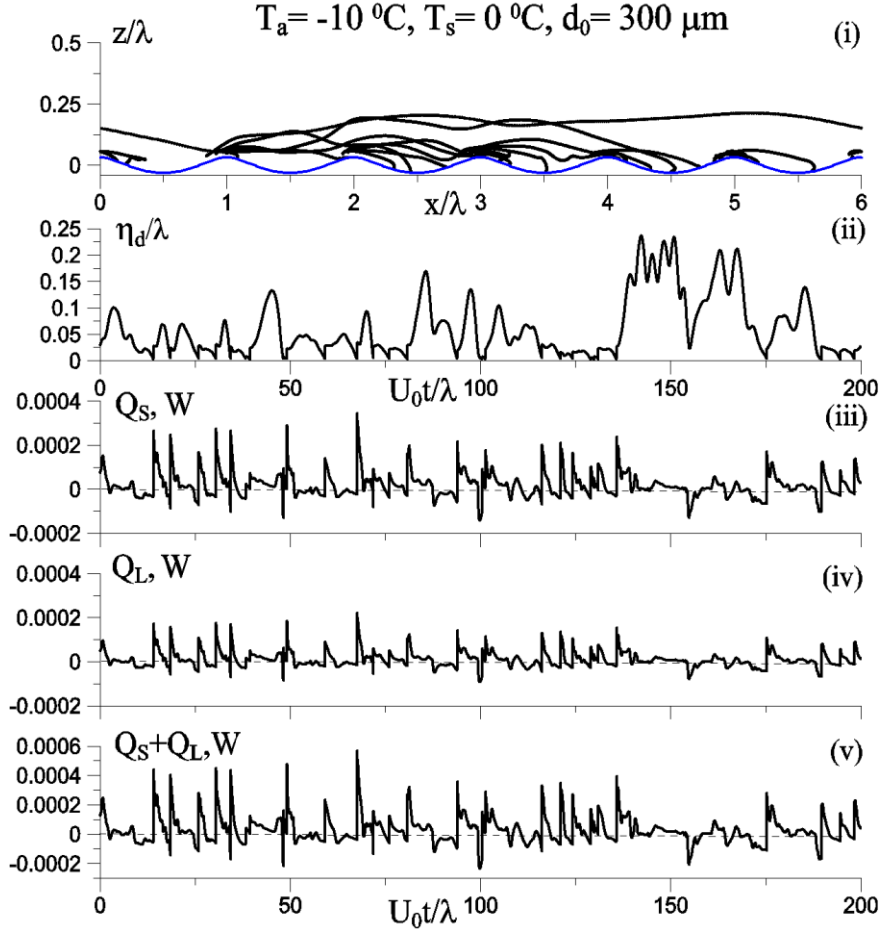


**Fig 6** The same as in Fig. 5 but for  $d_0 = 300 \mu\text{m}$ .

## Phase-averaged fluxes

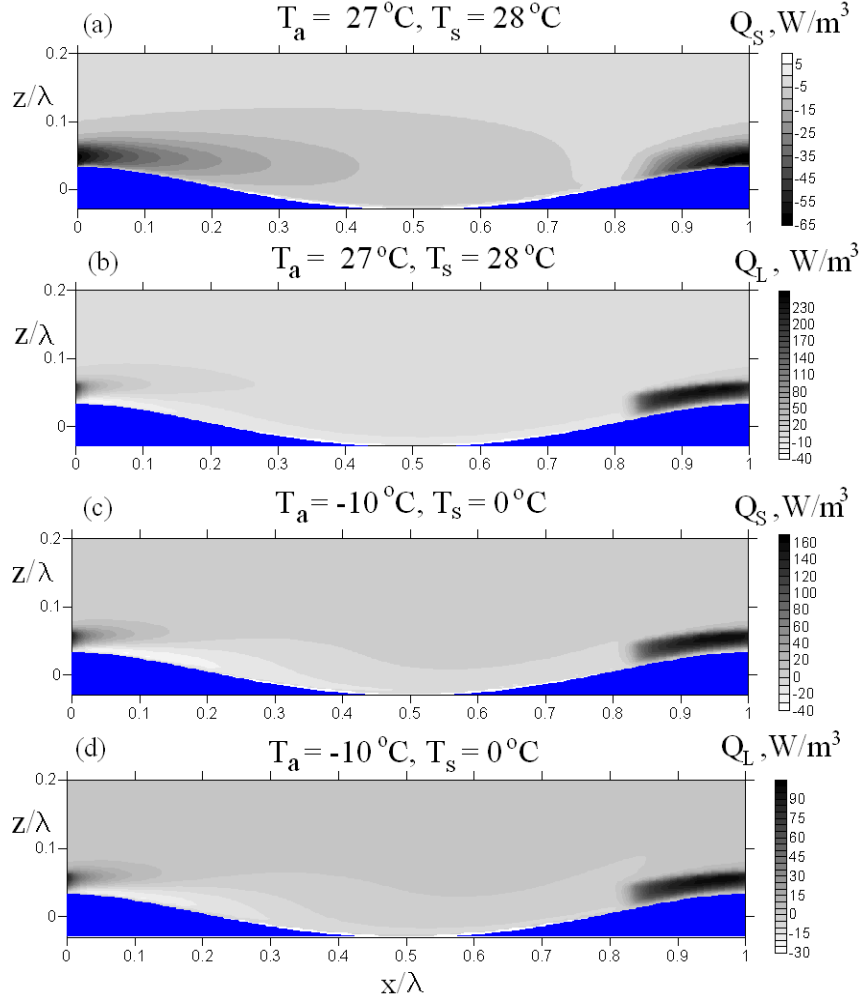


**Fig 7** Phase-averaged sensible (a,c) and latent (b,d) heat fluxes from the droplets to the air ,  $\langle Q_s \rangle$  and  $\langle Q_L \rangle$ . Panels (a,b) and (c,d) are for TC and PL conditions, respectively.

Phase-averaged fields of the droplets-mediated fluxes of sensible and latent heat per unit volume,  $\langle Q_s \rangle$  and  $\langle Q_L \rangle$ , evaluated as:

$$\langle Q_{s,L} \rangle = \sum_{n=1}^{N_d} Q_{s,L}^n \frac{w(r^n, r)}{\Omega_g}, \quad (5)$$

Figures 3-7 above show that sensible heat flux,  $\langle Q_s \rangle$ , is negative under TC conditions and positive under PL conditions whereas the latent heat flux,  $\langle Q_L \rangle$ , is mostly positive in both cases but is substantially reduced in the PL case as compared to TC case. Thus, as illustrated, droplets affect the carrier air flow in two opposite ways: under TC conditions, the droplets moisturize and cool the air whereas under PL conditions, the droplets mostly warm up the air.

## Mean profiles and size distributions: TC case

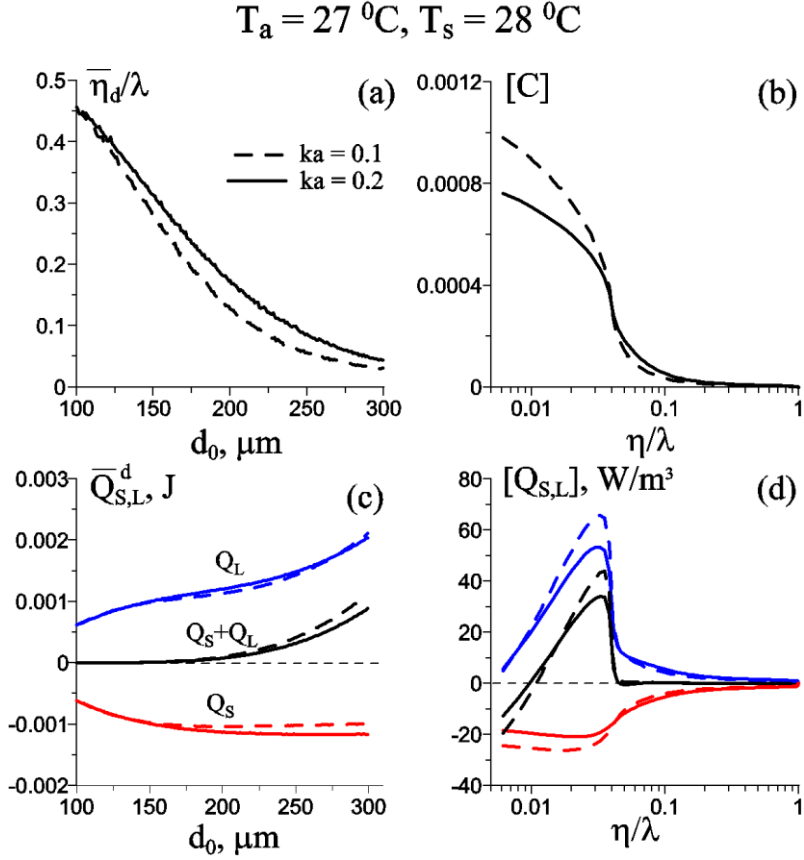


**Fig 8** Size distributions (left column) and mean profiles (right column) obtained under TC conditions: mean droplet height over water surface,  $\bar{\eta}_d$ , (a); droplets concentration, [C], (b); and sensible and latent heat and enthalpy transferred from droplet to the air,  $\bar{Q}_{S,L}^d$ , and  $\bar{Q}_L^d + \bar{Q}_S^d$ , (c) and the fluxes profiles  $[Q_L + Q_S]$  (red, blue and black colours, respectively), (d). Distributions  $\bar{Q}_{L,S}^d$  are obtained by integration over individual droplets Lagrangian trajectories and bin-averaging whereas the profiles  $[Q_{L,S}]$  are obtained by the summation over all droplets, phase-averaging and averaging over the wave length. Solid and dashed curves are for wave slope  $ka = 0.2$  and  $ka = 0.1$ , respectively.

Figure 6 shows that sufficiently large droplets (with diameter  $d_0 > 200\mu\text{m}$ ) are found mostly near the water surface, and mainly these drops contribute to the net enthalpy flux. Therefore, the flux peaks in the vicinity of the water surface, in the buffer region at  $\eta/\lambda \approx 0.03$  ( $\eta u_* \text{Re} \approx 15$ ). On the other hand, smaller droplets are found at larger distances from the water surface and in the "wet-bulb" state, and do not contribute to the enthalpy flux which therefore sharply decreases and almost vanishes at  $\eta/\lambda > 0.04$ . The fluxes are reduced with increasing wave slope,  $ka$ .

## Mean profiles and size distributions: PL case

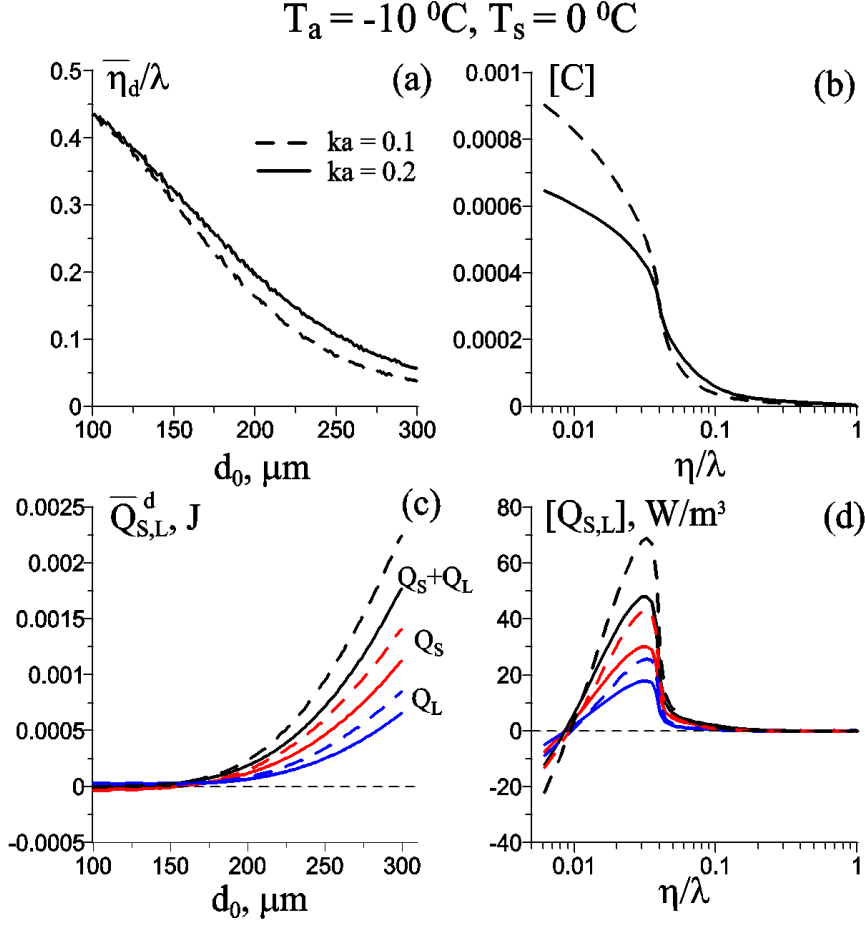


**Fig 9** The same as in Fig. 8, but for PL-conditions.

In the PL-case, the sensible heat,  $[Q_s]$  flux is positive and substantially larger than the latent heat flux,  $[Q_L]$ . It is important to note, that in the considered (PL) case, both  $[Q_s]$  and  $[Q_L]$  are positive, contrary to the TC-case (Fig. 8) where  $[Q_s]$  is negative, and the  $[Q_L]$ - peak in the PL-case (about  $17 \text{ W/m}^3$  for wave slope  $ka = 0.2$  in Fig. 7d) is substantially reduced as compared to the  $[Q_L]$ -peak in the TC-case (about  $50 \text{ W/m}^3$  for  $ka = 0.2$ ). The resulting peak of the enthalpy flux ( $[Q_s + Q_L]$ ) in the PL-case exceeds that in the TC- case by almost 30% ( $[Q_s + Q_L]_{peak} \approx 34 \text{ W/m}^3$  and in the TC case vs.  $[Q_s + Q_L]_{peak} \approx 48 \text{ W/m}^3$  in the PL-case for  $ka = 0.2$ ) due to the dominant positive contribution of the sensible heat flux.

## Conclusions

The results show that the droplet-mediated heat transfer observed in the tropical-cyclone (TC) case is distinctly different from that in the polar-low (PL) case. Under TC-conditions, the sensible heat flux from droplets to air,  $Q_S$ , is negative whereas the latent heat flux,  $Q_L$ , is positive, and thus droplets cool and moisturize the carrier air. This observation is in accord with earlier DNS results obtained under similar bulk parameters by Druzhinin et al. (2018). On the other hand, the results obtained under PL-conditions show that both  $Q_S$  and  $Q_L$  are positive, and  $Q_L$  – contribution is significantly reduced as compared to  $Q_S$  - contribution. The reason for the  $Q_L$  - reduction here is related to an exponential decreasing of the saturation vapour density at the droplet surface with reducing the surrounding air temperature. On the other hand, the sensible heat flux from droplets to the air,  $Q_S$ , is enhanced due to a larger temperature difference between the relatively warm droplet solution and the colder surrounding air. Thus in this, PL, case, droplets mostly warm up the air.

In both TC and PL cases, the droplet-mediated enthalpy flux,  $Q_S + Q_L$ , is positive, vanishes for sufficiently small droplets (with diameters  $d \leq 150 \mu\text{m}$ ) and further increases with  $d$ . Thus, only sufficiently large droplets contribute to the enthalpy transferred to the air. Since these droplets are found mostly in close vicinity of the water surface, the most of the enthalpy transfer from droplets to air occurs in the buffer region of the boundary layer. In the logarithmic region, only sufficiently small droplets (with diameters less than  $150 \mu\text{m}$ ) are found, and their contribution to the enthalpy transfer is negligible since these droplets for the most part of their lifetime are found in the "wet-bulb" state.

This work is supported by the Ministry of Education and Science of the Russian Federation (Task No. 0030-2019-0020). Numerical algorithms were developed under the support of RFBR (Nos. 18-05-60299, 18-55-50005, 18-05-00265, 20-05-00322). Postprocessing was performed under the support of the Russian Science Foundation (No. 19-17-00209).